X-716-67-350

NASA TM X- 55852

ANALYSIS OF THE ADVANCED NIMBUS POWER SYSTEMS

GPO PRICE $ _____

CFSTI PRICE(S) $ _____

Hard copy (HC) 3.00

Microfiche (MF) .65

ff 653 July 65

JULY 1967

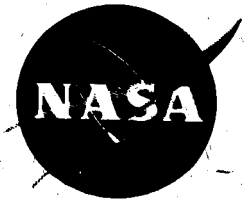

GODDARD SPACE FLIGHT CENTER

GREENBELT, MARYLAND

X-716-67-350

ANALYSIS OF THE ADVANCED NIMBUS POWER SYSTEMS

Charles N. Bolton
Space Power Technology Branch, GSFC

and

Paul S. Nekrasov
RCA Astro-Electronics Division

July 1967

GODDARD SPACE FLIGHT CENTER
Greenbelt, Maryland

ABSTRACT

The solar-conversion power-supply subsystem to be flown on the Nimbus B spacecraft in the first quarter of 1968 will be the second generation of power supplies for the Nimbus mission.

This second-generation power supply, capable of delivering regulated loads between 50 and 500 watts in a 600-n. m. high score sun-sync orbit, includes improved methods of charge regulation, in addition to the use of the advance voltage regulator (AVR), a pulsewidth-modulated (PWM) regulator developed for NASA/GSFC by RCA under contract NAS-5-3248.

The use of a PWM regulator requires a detailed system analysis which includes the investigation of multiple operating points and lockup. A generalized approach to investigating multiple operating points, followed by a detailed analysis, indicates that there are no series lockup modes for the Nimbus B mission.

The reason for a new generation of power-supply subsystems is to take advantage of major advances in the state-of-the-art. The first-generation power-supply subsystems used dissipative series-voltage regulators. As a follow-on to the more efficient advance voltage regulator on the second-generation Nimbus B mission, a third-generation concept of Nimbus power-supply subsystems is being investigated which includes the most recent advances in power-conditioning technology, known as maximum power-point tracking. Comparison of Nimbus B with the several system approaches to maximum power-point tracking reveals possible advantages from this mode of operation.

CONTENTS

ILLUSTRATIONS

ANALYSIS OF THE ADVANCED NIMBUS POWER SYSTEMS

Charles N. Bolton
Space Power Technology Branch, GSFC
and
Paul S. Nekrasov
RCA Astro-Electronics Division

INTRODUCTION

The Nimbus B satellite, which will be designated Nimbus 3 when in orbit, will be launched in the first quarter of 1968 (Figure 1). Nimbus 1 and Nimbus 2 were launched successfully in August 1964 and May 1966 respectively.

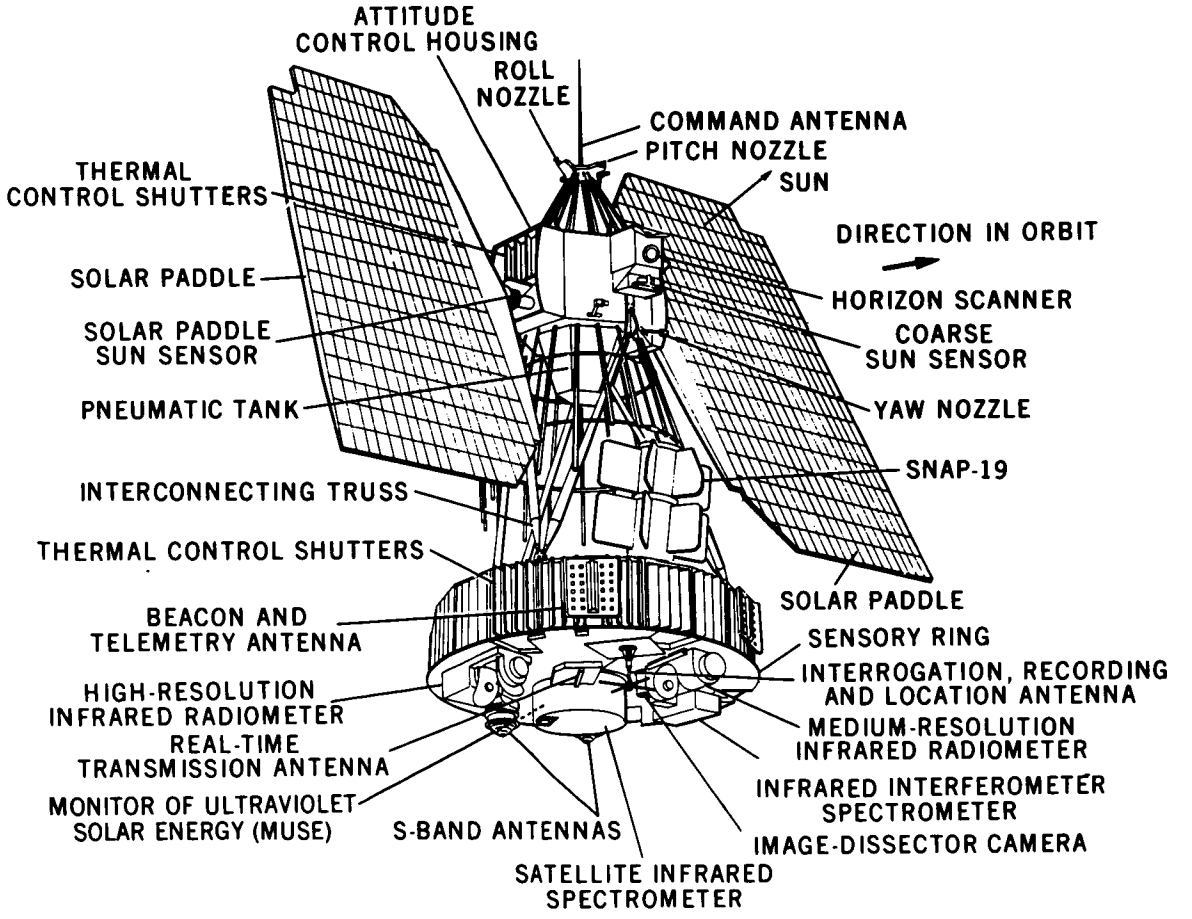

Figure 1. Nimbus B Spacecraft Configuration

The objective of the Nimbus program is to develop an observatory-satellite system capable of meeting the R&D needs of the nation's atmospheric scientists and weather services, and to provide global surveillance of atmospheric structure from orbital altitudes. To meet this objective, Nimbus B will be launched into a nominal 80-degree retrograde circular orbit at an altitude of 600 nautical miles (Figure 2). The spacecraft will be three-axis-stabilized, the yaw axis always being aligned with the earth's local vertical. The orbital plane will be close to the earth-sun line so that the spacecraft will always pass over head around local noon or midnight. The solar paddles are controlled to maintain their solar-cell surface perpendicular to the sun line throughout the day portion of each orbit.

The modular design of Nimbus (Figure 3) distributes the batteries, regulators, and associated electronics among several of the 18 bays constituting the sensory ring and connects them to the solar array through sliprings located in the stabilization and control housing. An active thermal-control system maintains the sensory ring at an average temperature of 25° C. Predicted paddle temperatures swing from a nighttime low of -74° C to a daytime high of +50° C.

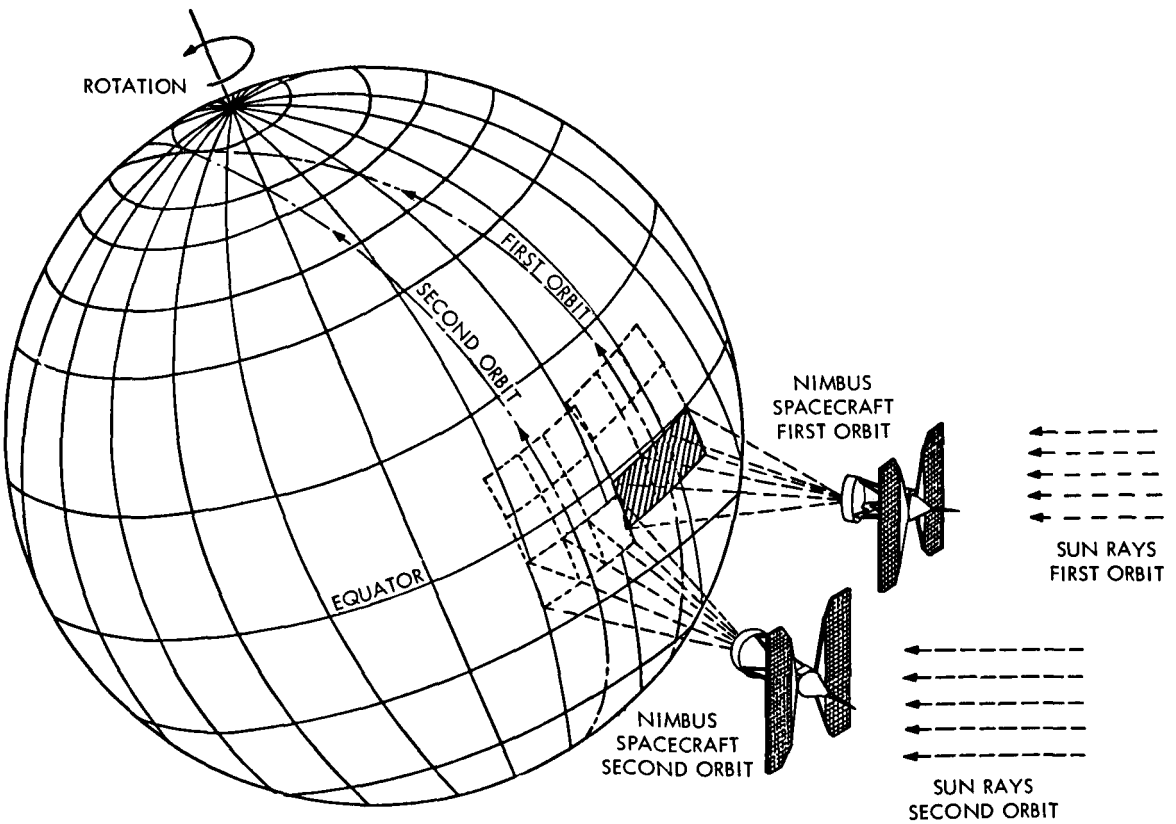

Figure 2. Nimbus B Orbit

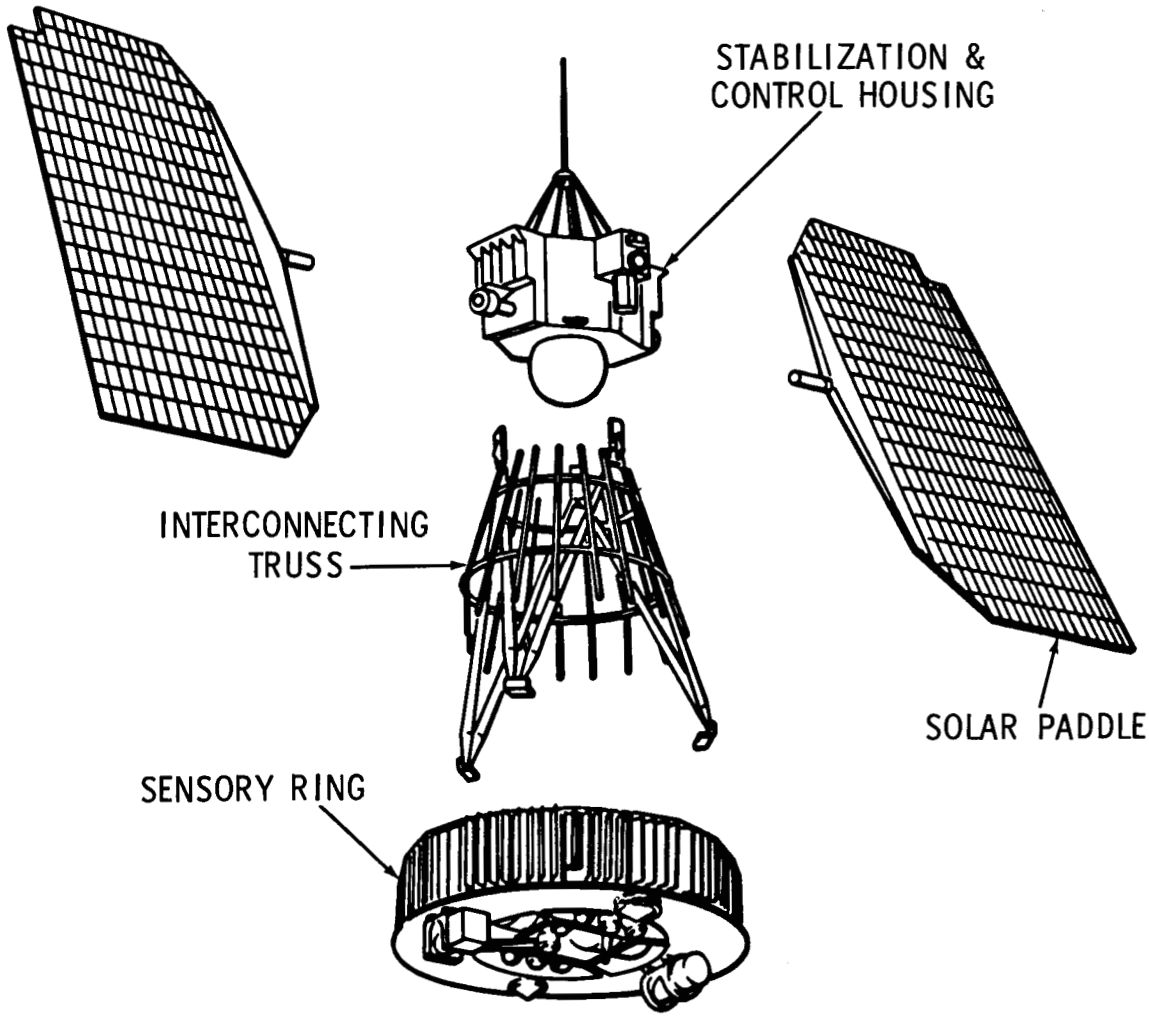

Figure 3. Nimbus Module Design

The Nimbus B power supply subsystem will use about 48 square feet of solar array to deliver an average satellite day-and-night power of more than 210 watts to spacecraft experiments and housekeeping subsystems. The experiments will measure the earth's radiation over wide regions of the electromagnetic spectrum, including ultraviolet and infrared, and will perform daytime TV cloud-mapping and data collection and ranging. The power, regulated at -24.5 volts ±2 percent at a main regulated bus, must be continuous: loss of the regulated voltage for more than 5 minutes will cause mission failure. Power supplied by the solar-conversion power-supply subsystem will be augmented by 50 watts of unregulated power supplied by radioisotope-fueled thermoelectric generator (RTG) units. The RTG's, to be used only for the Nimbus B satellite, will be physically mounted together and attached to the top of the sensory ring.

The power-supply subsystem on Nimbus B is a second-generation development, the power-supply subsystems flown on Nimbus 1 and Nimbus 2 being the first generation. The generation to be flown after Nimbus B is now being investigated. The Nimbus 1 and Nimbus 2 missions had average continuous-load power requirements in the 165-watt range, using a dissipative series-pass-type main bus-voltage regulator. The average continuous-load power requirements of the Nimbus B spacecraft will be about 230 watts, and the subsystem will include improved methods of charge control and a pulsewidth-modulated down-converter-type main bus-voltage regulator. Spacecraft requirements for the third generation of power-supply subsystems will be in the 350-watt or greater range; techniques under investigation in this area include the advanced concept of maximum power-point tracking.

The continuous effort throughout the development of the Nimbus power-supply subsystems has been to make the transition from one generation power supply to the next as logical and smooth as possible, and at the same time to maintain the capability of meeting the increasing needs of the Nimbus program.

THE NIMBUS POWER SYSTEMS

The basic concept (Figure 4) of the solar-conversion power-supply subsystems for the Nimbus satellite has remained the same for the first and second generations: several batteries operating in parallel, and one main regulated

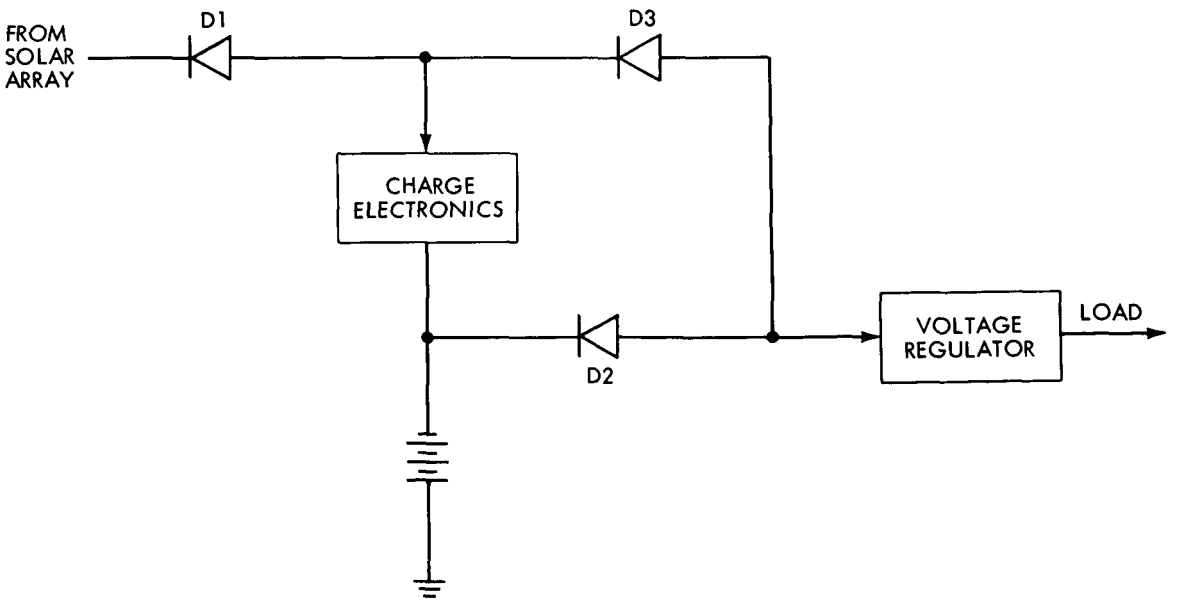

Figure 4. Block Diagram, Nimbus Power Subsystem

bus fed by an oriented solar array. The third generation is not expected to deviate significantly from this concept.

The major improvements, from one generation to the next, have taken place at the component or black-box level and in the method of interconnecting the components. The prime source of electric energy is an array of solar cells located on two panels normally oriented to the sun. Each of the several nickel-cadmium storage batteries is packaged in a separate battery module in a 23-series-cell configuration. Charge electronics regulates the charge current, protects each individual battery, and performs certain additional functions in an advanced version of this circuit. Depending on the specific Nimbus power-system concept, the voltage regulator is either of the dissipative series-pass type, or a pulsewidth-modulated (PWM) down-converter. In either case, it delivers rated load current at -24.5 ±0.5 volts.

During sun-illuminated flight, the solar array charges the batteries through charge electronics and delivers load power to the voltage regulators. During eclipse, the batteries deliver load power through discharge diodes D2. Diodes D2 and D3 serve to isolate the several individual batteries electrically; D2 also protects the battery from receiving uncontrolled charge.

The first-generation Nimbus power system included dissipative current-limiter charge electronics and dissipative series regulators, shown in block diagram form in Figure 5. Regulated voltage V_R is maintained by controlling the voltage magnitude across the series-element transistor Q1. Regulated voltage magnitude is compared to a fixed reference voltage; error voltage is detected, amplified, and delivered to the Q1 as a change in base drive of appropriate magnitude and direction. Because the input voltage V_{in} is derived from the solar array and battery, V_{in} is variable and any voltage difference between that and V_R appears as a voltage drop across Q1. During charge, V_{in} can be as large

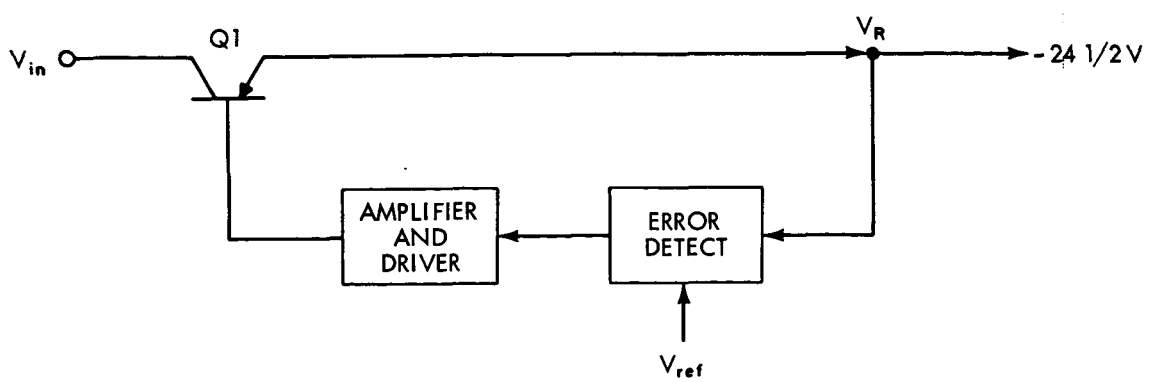

Figure 5. Dissipative Series Regulator

as 1.5 V_R in a nickel-cadmium battery system, resulting in poor load-regulation efficiency of the order of 65 percent or less.

Application of the advanced voltage regulator (AVR) to the second-generation Nimbus power system scheduled for flight in 1968 has appreciably improved regulation efficiency. The AVR, which uses PWM techniques, has a block diagram similar to that of the series regulator (Figure 5), except that the base drive delivered to Q1 is in the form of a series of pulses whose duty cycle α is controlled. Figure 6 shows the details of the circuitry associated with Q1, shown here as a duty-cycle-controlled switch. Input filter L1-C1 delivers power to Q1 when ON and maintains continuous flow of the source current to the regulator. L2-C2 is an output filter designed to minimize the load bus ripple induced by the ON-OFF operation of Q1. CR1 is a flyback diode which provides continuity for the load current flow (I_L) maintained by L2 during Q1 OFF time. It can be shown* that the dc input-output voltage relationship is, approximately,

$$V_R = \alpha V_{in}$$

If V_{in} increases as it will during charge, the duty cycle α is reduced to maintain a fixed output voltage V_R. Reduction of the ON-time duty cycle will be followed by a reduced I_{in} magnitude, in such a way as to maintain any given product V_{in} I_{in} relatively constant for a given fixed load $V_R I_L$. The AVR, therefore, has a reasonably constant efficiency factor associated with it: source-voltage fluctuations at V_{in} level do not impose an undue penalty on the efficiency of regulation, as they do in a dissipative series regulator.

A new concept based on PWM techniques, now under investigation, will when completed become part of the third-generation Nimbus power-system design.

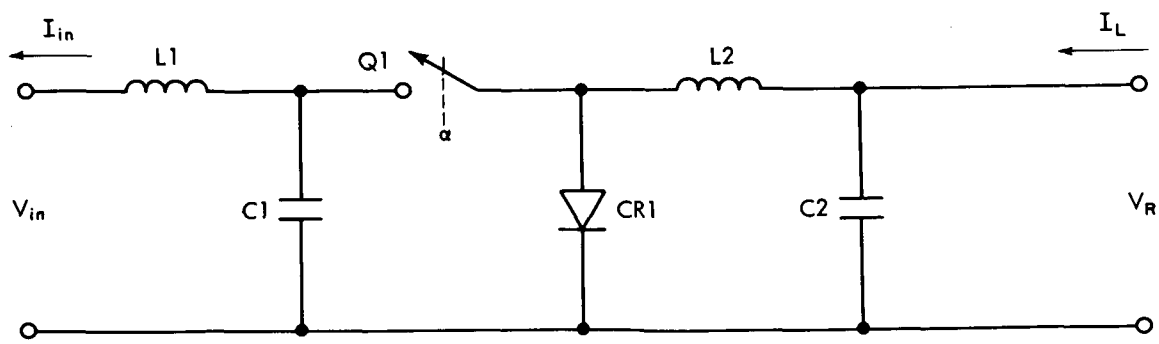

Figure 6. Duty-Cycle-Controlled Switch and Associated Circuitry

*C.M. Mackenzie, R.C. Greenblatt, A.S. Cherdak. Nimbus Power Systems. NASA document X-450-66-333.

The concept is based on replacing the present dissipative charge electronics by a modified AVR whose duty cycle would be controlled to maintain a particular input voltage, rather than to keep a constant output voltage. *

It is known that, for any given set of environmental conditions, a solar array will deliver maximum power when operated at a particular voltage. Figure 7 illustrates a typical power-voltage relationship in a solar array. If a substantial portion of the array output is delivered through an AVR into a source of relatively fixed voltage, such as a battery under charge, the AVR's duty cycle could be adjusted continuously to maintain $V_{in} = V_{max}$ (array).

This technique, known as maximum power-point tracking, results in the solar array's delivery of the maximum energy possible per-orbit. The duty

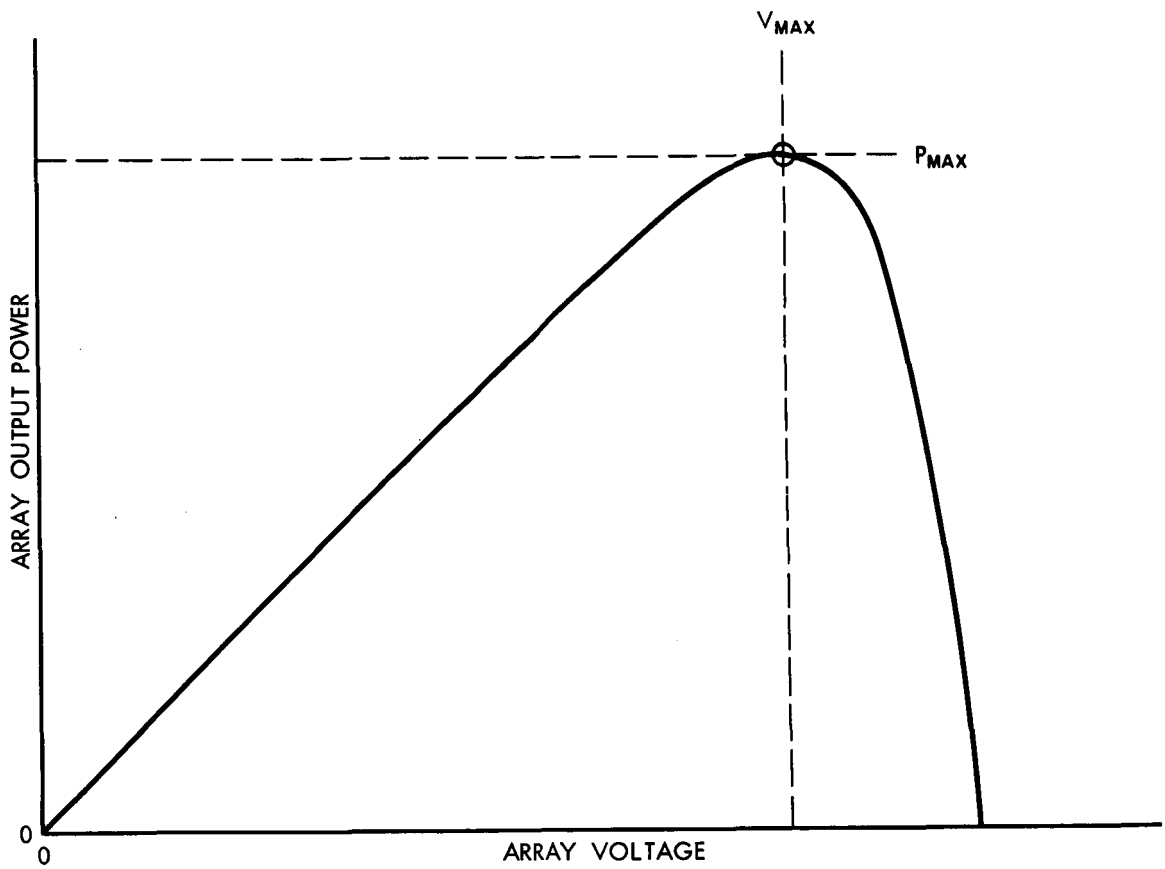

Figure 7. Solar-Cell Array Power vs Voltage Characteristic

*P. Nekrasov. Systems Comparison and Analysis of Tracking and Non-Tracking Space Power Supplies. Fourth Space Congress, Cocoa Beach, Florida. April 1967.

cycle can be adjusted to any value within a reasonable range, and the array can be operated at any power point less than P_{max} if required, thereby greatly reducing internal peak-power dissipation. This technique also removes the necessity to match the array-output characteristic closely to the remainder of the power system, a critical design consideration in nontracking systems.

DETAILED ANALYSIS OF THE NIMBUS B POWER SYSTEM

The second-generation version of the Nimbus power system, to be flown in 1968 on the Nimbus B spacecraft, includes an AVR load-voltage regulator whose efficiency vs load plots are approximately as shown in Figure 8, and an improved dissipative charge-electronics/current-limiter circuit with a voltage-current characteristic as shown in Figure 9. Other significant component data include a voltage-limiter threshold-voltage characteristic (Figure 10), nominal end-of-life i-v curve of a typical Nimbus B nickel-cadmium storage cell (Figure 11), and the solar-array output characteristic based on worst-case design criteria at the predicted steady-state cell temperature of +40° C (Figure 12).

This section contains a detailed analysis of the system. The advanced voltage regulator (AVR) input terminals were selected as the most convenient reference point for evolving the details of the analysis. At that point, it is most convenient to investigate the power-system output capability, and compare it with load demand which appears at AVR terminals as a family of curves approximating hyperbolas on an I-V plot. The analysis will reflect exact operating conditions insofar as possible, approximations being made only to the extent that it is desired to examine the system in a state of typical (rather than possible) conditions of life, temperature, and state of charge.

Figure 13 is a redrawing of the block-diagram configuration (Figure 4) to show specific conditions applicable to Nimbus B. Figure 13 shows only one battery, although the actual system contains eight battery modules. Expressed on a per-module basis, the system is subject to the following shunt-current drains: 22 ma at voltage V_S, 22 ma at V_B, and 25 ma at V_R. These currents are required to operate the power system electronics, and, to the extent that they are not delivered as either load or charge, are considered as a loss.

The following analytical procedure was used to determine the end-of-life power-system output characteristic at AVR input terminals.

Solar Array

Referring to Figure 14, the array output at cell level (array side of blocking diodes D1) is as shown in Figure 12. To reflect true conditions at AVR input

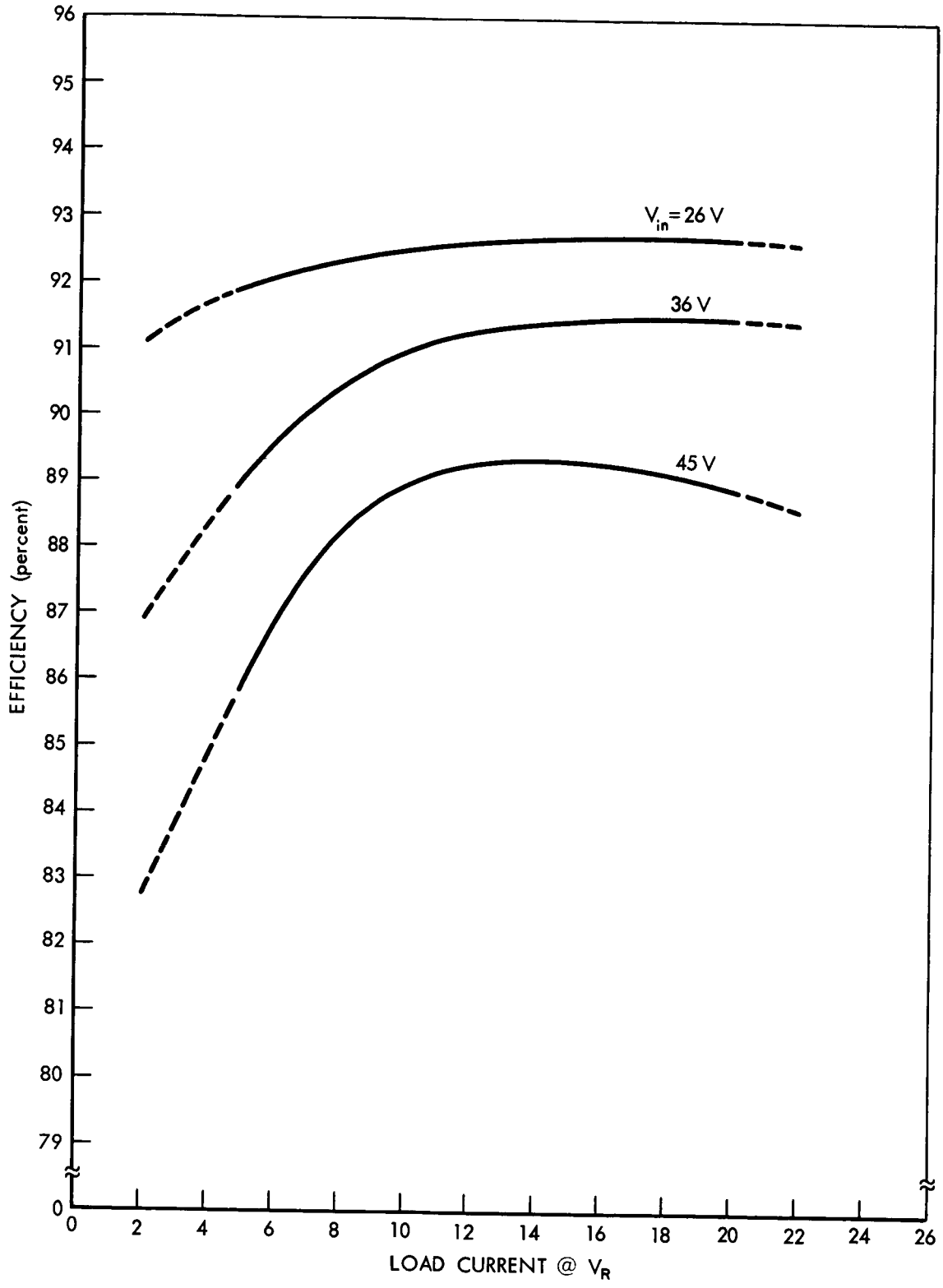

Figure 8. AVR Efficiency vs Load at +25°C

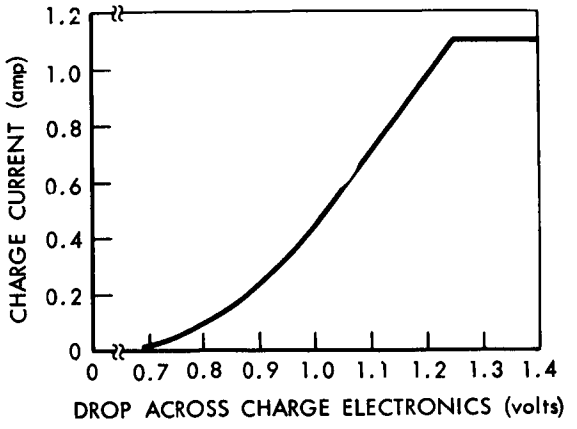

Figure 9. Nominal Charge Electronics, Limiting Characteristic

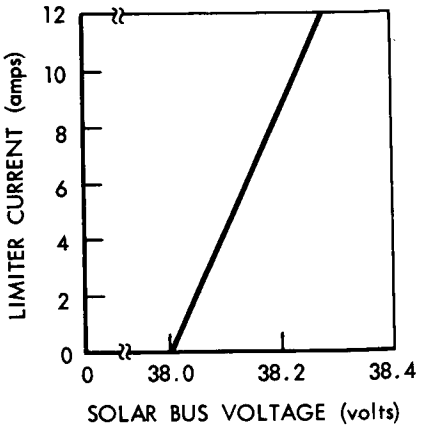

Figure 10. Voltage Limiter vs Threshold Voltage

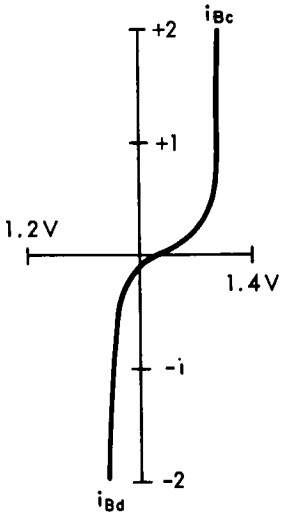

Figure 11. Typical Nimbus B Ni-Cad Storage Cell

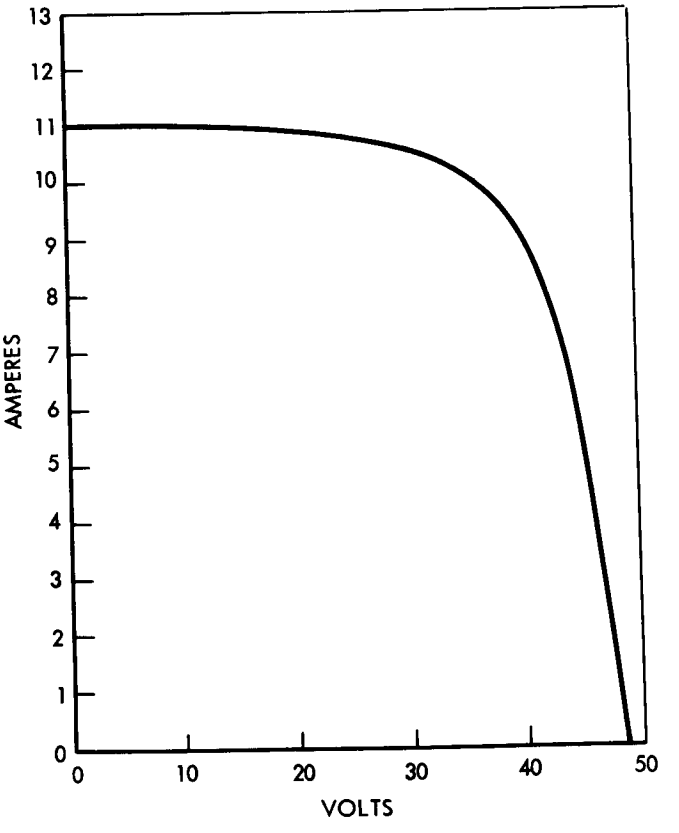

Figure 12. Worst-Case Predicted Output of Nimbus B Solar Array (+40°C, 12 months in orbit)

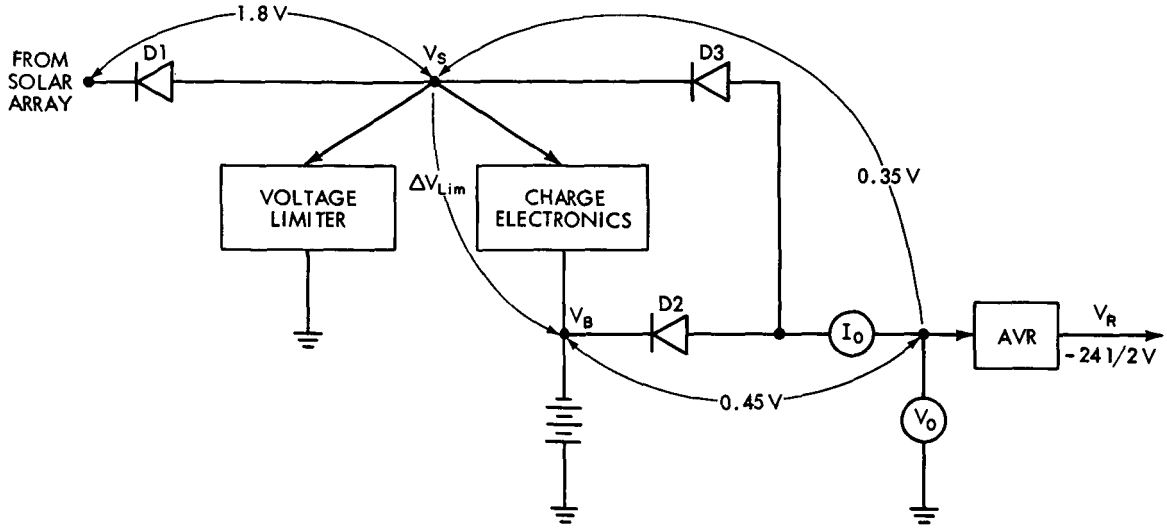

Figure 13. Simplified Diagram, Nimbus B Power Subsystem

(I_O, V_O, Figure 13), the following shifts are applied to the solar-cell output curve over the significant voltage range of power-system operation:

- Voltage shift—Entire curve is shifted to the left by amount 1.8 + 0.35 = 2.15 volts, the total voltage drop from solar cells to AVR input terminals.

- Current shifts—First, entire curve (shifted as above) is further shifted downward by the amount of total shunt loss at V_S (i.e., 22 ma x 8 modules = 0.176 amp). Second, part of the resultant curve from battery open-circuit voltage and to the right, is shifted by the amount of total loss at V_B, or by another 0.176 amp.

The array output characteristic thus shifted is further altered to reflect the shunt limiter. The nominal shunt-limiter characteristic (Figure 10) shows the circuit turning ON at 38 volts; reflected to AVR terminals, the turn-on voltage is reduced by the drop thru the D3 diode path, i.e., 38 - 0.35 = 37.65 volts. At AVR input terminals, then, the array output is limited at turn-on to that voltage, and is labeled "s" in Figure 11 where a curve can now be drawn thru points i-o-s to show the reflected array output.

Point "s" in Figure 14 is located at I_O = 8.6 amperes, corresponding to 38.2 volts on the nominal shunt limiter characteristic. At AVR input, this becomes 38.2 - 0.35, or 37.85 volts shown as point "v" in Figure 14 where the reflected effective array output is now completed as i-o-s-v.

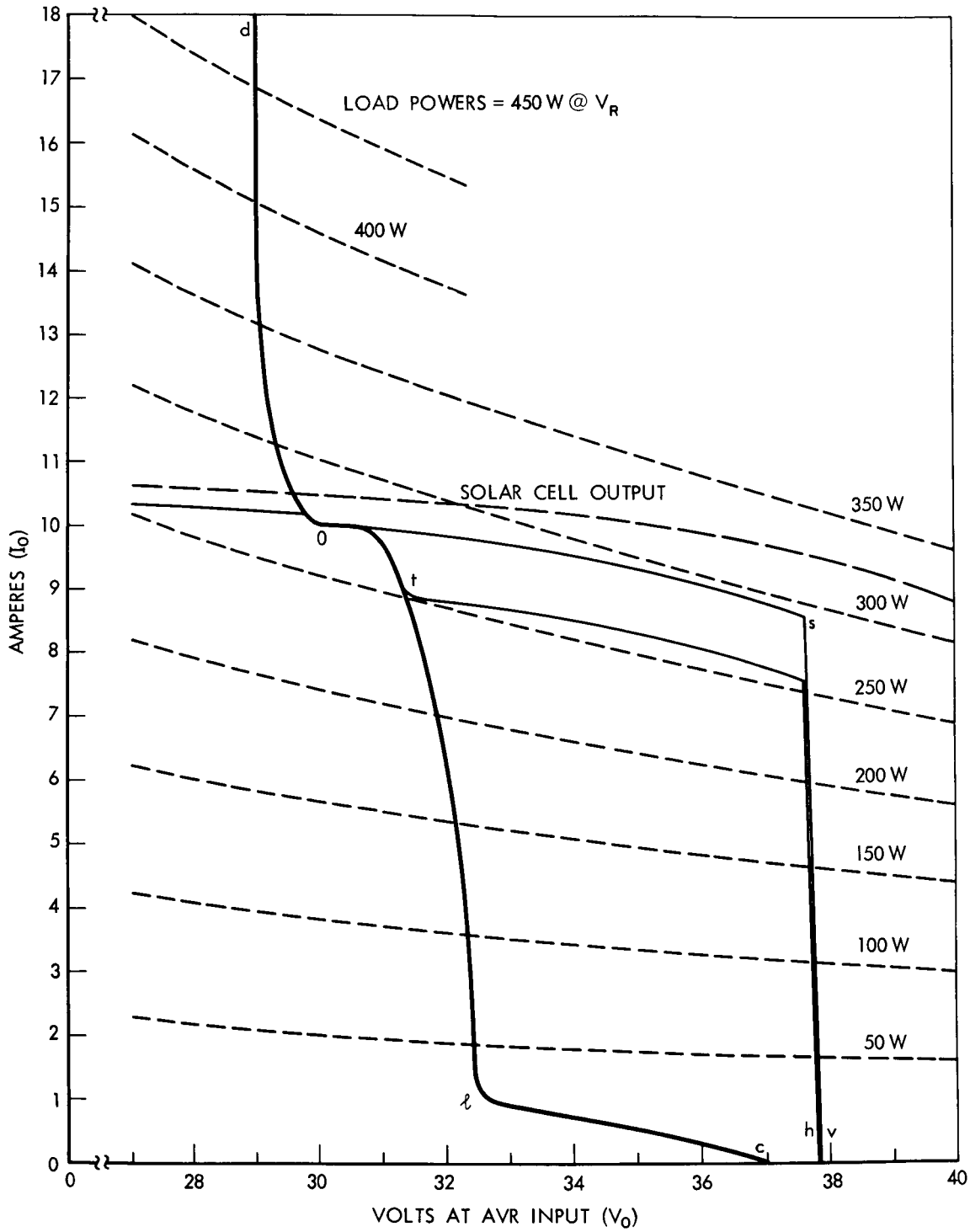

Figure 14. End-of-Life (12 months) Nimbus B IV Characteristics at AVC Input

Reflected Discharge Characteristic

Three items are significant: First, the battery discharge voltage is reduced at AVR input by the amount of voltage drop thru the D2 path (i.e., by 0.45 volts); second, there are 23 storage cells in series; third, when in discharge, the eight batteries deliver a shunt loss at V_B of 0.176 amps total.

In the following tabulation, the first two columns are the discharge voltage and current of a nominal Nimbus B storage cell (Figure 11), the third column is the voltage at AVR input, and the last column is the net total current through the discharge path D2:

V_{Bd} (volts per cell)	i_{Bd} (amperes)	V_o* (volts)	I_o** (amperes)
1.318	0	29.85	
1.295	0.15	29.3	1.02
1.283	0.4	29.1	3.02
1.28	0.6	29.0	4.62
1.279	0.7	28.95	5.42

*$V_o = 23\ V_{Bd} - 0.45$ volts
**$I_o = 8 i_{Bd} - 0.176$ amp.

Discharge characteristic o-d is generated in Figure 14, by graphically adding current values in the last column to i-o, at corresponding voltages.

Reflected Battery Charge and Charge Electronics Characteristics

In the tabulation below, the first two columns are the per-cell charge voltages and currents from Figure 11; the third column is the voltage difference between the charge electronics input and the battery terminals corresponding to charge current i_{Bc}, taken from the nominal charge electronics characteristic, Figure 9. The fourth column is the charge electronics input voltage V_S reflected to the AVR input (i.e., the sum of battery charge voltage and limiter drop is reduced by the drop thru D3). The last column is the total battery charge current.

Overall characteristic tabulated in the last two columns is constructed in Figure 14 by subtracting 8 i_{BC} from o-s at corresponding voltages, whereupon

V_{BC} (volts per cell)	i_{BC} (amperes)	$\Delta V_{lim.}$ (volts)	V_o* (volts)	8 i_{BC} (amperes)
1.318	0	0.7	30.7	
1.342	0.16	0.85	31.35	1.28
1.36	0.35	0 96	31.9	2.8
1.366	0.54	1.04	32.1	4.32
1.368	0.77	1.13	32.3	6.16
1.37	1.10	1.25	32.45	8.8

*$V_o = 23\ V_{BC} + \Delta V_{lim} - 0.35$ volts

Bottom row in the table represents the current limiting condition.

curve o-1 is drawn. Beyond point "I", the characteristic is obtained by subtracting the limiting value of 8 i_{BC} (i.e., 8.8 amps) from o-s-v. The entire power-system output characteristic during charge is thus o-l-c.

Similarly, o-t-h is drawn to show trickle-charge condition (that is, one where the total charge to all eight batteries is assumed to be limited to 1 ampere).

The entire power-system output characteristic as seen at the input to the AVR, or any other regulator, is d-o-l-c. Method of construction of the beginning-of-life characteristic d'-o'-l'-c' in Figure 15 is identical in every way to that outlined above.

Construction of Fixed Load Lines at AVR Input

The AVR input current I_o equals

$$I_o = \frac{P_L + P_{loss}}{e_c\ V_o}$$

where P_L is load power, watts, at the regulated bus voltage V_R = 24.5 volts
P_{loss} is the shunt current loss at V_R expressed at 25 ma per module x 8 modules x 24.5 volts, or about 5 watts
e_c is the AVR efficiency factor (Figure 8)
V_o is the AVR input voltage

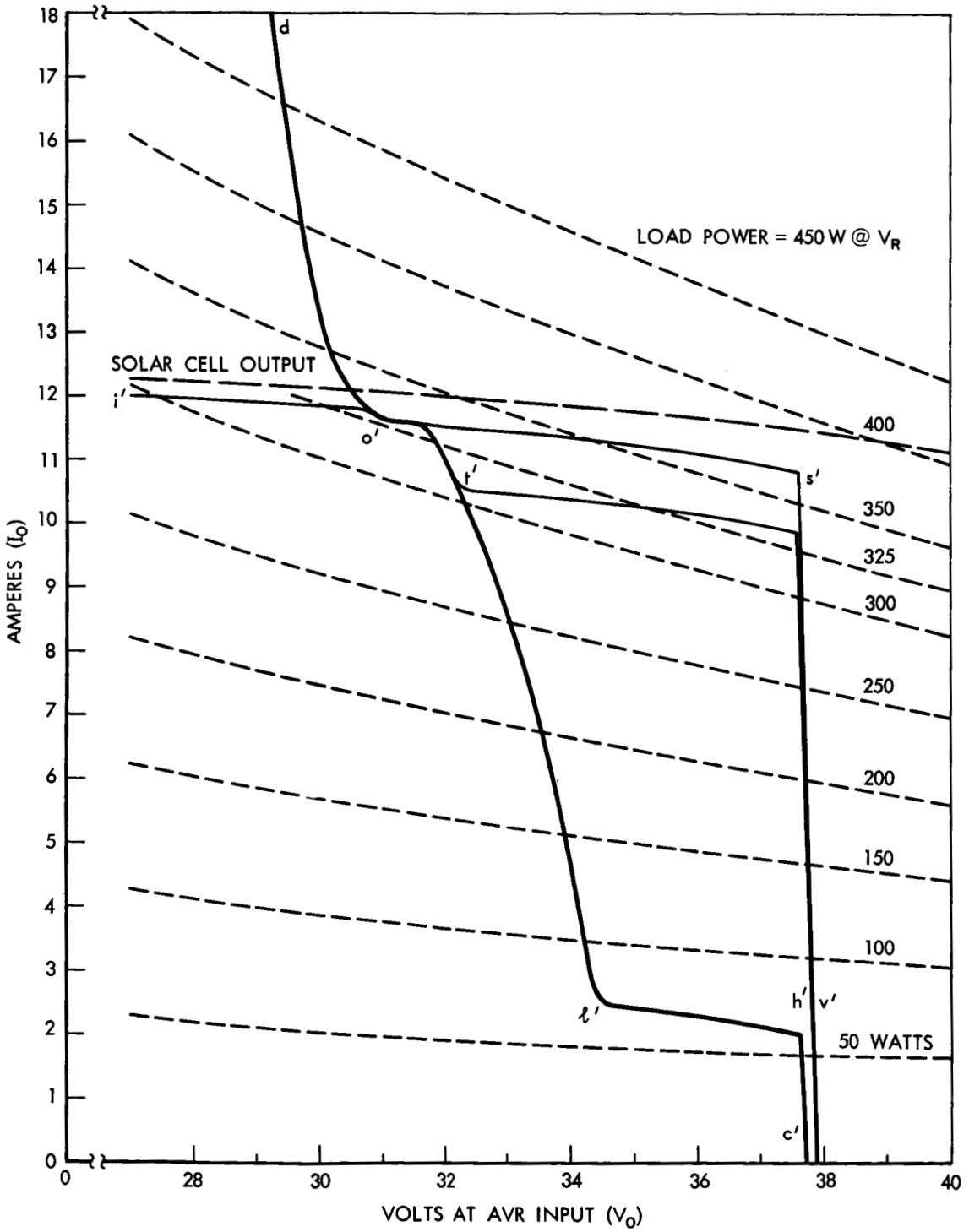

Figure 15. Beginning-of-Life Nimbus I-V Characteristics at AVC Input

Values of V_o, I_o are plotted in Figures 14 and 15 (dotted curves) for fixed loads P_L in 50-watt steps.

MULTIPLE OPERATING POINTS AND LOCKUP

The analysis performed in the preceding section produced results which have been used to investigate certain specific problem areas occurring in power subsystems which use pulsewidth-modulated voltage regulators. A possible problem known as "lockup" will be described in general terms, followed by the application of the analysis developed, to determine whether any undesirable phenomena can occur in the Nimbus B power subsystem.

It has been known for some time that constant-power load requirements of certain magnitudes can be satisfied by more than one point on the power-system output characteristic.* In many cases, it can be shown that certain fixed load lines intersect the output characteristic twice, three times, even five times. Assuming that a power system can be operated on any part of its I-V output characteristic (the only limitation being that the required load power equals source power availability), there are as many possible operating points as there are intersections.

The problem of lockup is frequently mentioned in conjunction with the possibility of multiple operating points. Where several operating points are possible, some are usually less desirable than others: for instance, a constant-power hyperbola may intersect the output I-V characteristic in the battery charge voltage region at one point, and in the discharge voltage region at another; the latter would be clearly the less desirable, or lockup, condition resulting in a less favorable condition of spacecraft energy balance.

The simplified sketch (Figure 16) is drawn to examine various multiple-operating-point possibilities. The solar-array output characteristic is defined by curve I_{sc}-o-b-v_{oc}, the battery discharge characteristic by o-d, and the battery charge plus limiter by o-l-c (or, by o-t-h showing a lower limiter setting, for a subsequent illustrative purpose), where charge limiting occurs on the l-c (t-h) part of the curve.

The power-system output characteristic at PWM regulator input is d-o-l-c. The load characteristics at the same point in the power system are shown by

*T.W. Koerner, "Static Power Conversion for Spacecraft", Astronautics and Aerospace Enginnering, May 1963

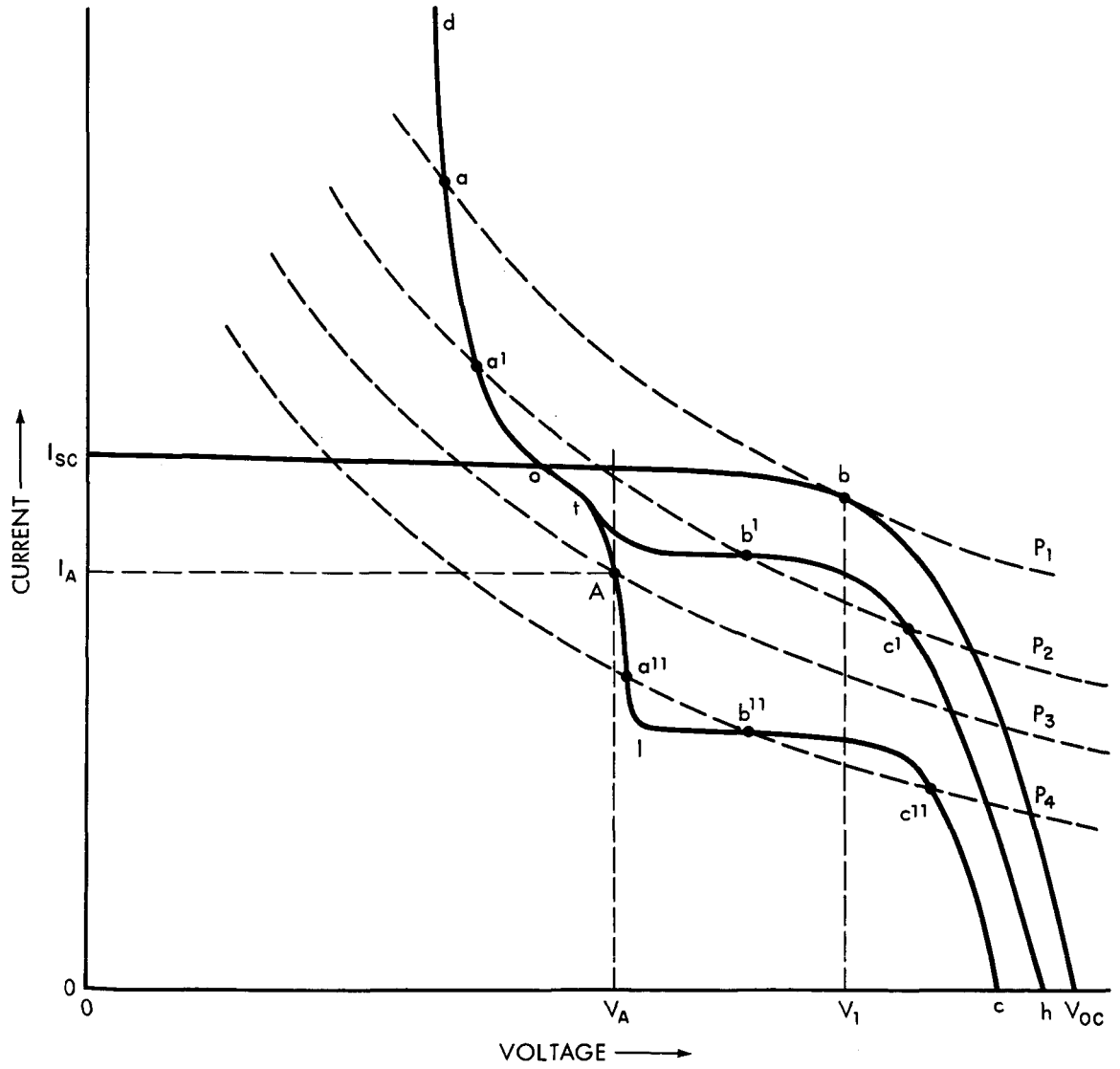

Figure 16. Multiple Operating Points

constant-power lines $P_1 > P_2 > P_3 > P_4$. The possible power system operating points at regulator input are defined as the points of intersection of a load line with d-o-1-c.

Returning to the sketch, load demand P_3 results in a hyperbola which intersects the power-system output characteristic d-o-1-c just once—at point A—and there is, therefore, no question that the regulator input voltage V_o equals V_A and the input current $I_o = I_A$, that the battery is under charge, and that the charge current is the difference between the array current at V_A (equal roughly to I_{sc} on this sketch) and I_A, subject to the simplifying assumptions of ideal diodes and negligible power-system shunt losses.

A different situation is encountered if the power demand is P_4, because the P_4 load line intersects the power system output characteristic three times: i.e., at a", b", and c". Assuming for the present that all three operating conditions are equally likely, b" and c" are essentially the same to the extent that in each case the charge electronics is limiting, allowing maximum recharge in either case. The third possibility is a": the battery is still under charge, but the charge electronics is not limiting, meaning that the amount of recharge is lower than at either of the other two possible operating points. Operating at a" is thus less advantageous, and, if operated there, the power system is considered to be in a state of minor lockup.

To illustrate a more drastic condition of lockup, let the power system characteristic be d-o-t-h instead, and let the power demand be P_2. In the previous example (P_4 and d-o-l-c), the difference between the desired operation and lockup was more, or less, charge respectively; charge occurred in either case. In the example being considered (P_2 and d-o-t-h), both b' and c' mean full charge, as did b" and c", but a', unlike a", means battery discharge. It is thus less desirable to be in a lockup condition such as a', compared to a".

Finally, let the power demand at the PWM regulator input be P_1, so that the load requirement just matches the solar array capability as shown by point b. Unlike the last two cases discussed, point a is not an example of lockup because it is the only point where the system can operate if the demand is P_1. Even though the array is capable of supplying P_1 at voltage V_1, presence of V_1 at the input of a series-pass dissipative limiter of the type commonly used would cause the flow of charge current equal to the current difference between curves c-v_{oc} and o-l-c (or o-t-h) at V_1. Diversion of some of the array output to the battery would result in the available load power's being something less than P_1, and the regulator action would kick the operating point over to "a", causing the battery to discharge. Stated a different way, a possible operating point exists only where the load line intersects the power-system output characteristic, such as at d-o-l-c, provided both are drawn to reflect conditions at the same point of the power system.

The foregoing discussion attempted to show what is, and what is not, considered a possible lockup condition. A distinction was made between two cases of lockup: One, where the recharge is merely lower than indicated by the source capability; the other, where the ability of the power system to both supply the load and charge the battery is not fully utilized, resulting in a net discharge instead.

Let Figures 14 and 15 be reviewed in light of the preceding discussion. Figure 15 shows the beginning-of-life conditions. When all batteries are

capable of being fully charged, the power system output characteristic is d'-o'-l'-c'. For all practical purposes, none of the fixed load lines intersects this characteristic more than once; therefore, chances of any lockup under the conditions shown are apparently nil.

As the batteries become recharged and the battery charge controllers are reduced, one by one to trickle charge the l'-c' portion of the output characteristic will move up and multiple intersections will occur (given fixed loads of around 250 watts or more) until all eight batteries are in trickle charge, at which time the system output characteristic will be d'-o'-t'-h'. Figure 12 shows that the 325-watt load line intersects the latter three times, raising the possibility of a "minor lockup" as for the P_4 condition at a" in Figure 16. It is significant to note that the lockup conditon described is not likely to occur until most of the batteries in the system are fully charged.

Figure 14 shows the end-of-life conditions. Close examination of the plots shows an even smaller chance of lockups than at the beginning-of-life, primarily because of the decreased voltage capability of the degraded array.

Based on the specific operating conditions examined, there appear to be few, if any, possibilities of a lockup of any significance in the Nimbus B power subsystem. Chances of what has been described as a minor lockup appear to be influenced mostly by the slope of the charge-controller characteristic when limiting, relative to the slope of the nearest fixed-load line. Most favorable conditions for this type of lockup occur when the limiting portion of the charge controller characteristic is horizontal, as in Figure 9, and when operation is carried on along the constant-current part of the array curve. Specifically, conditions under which undesirable operation could occur apply over a range of loads bounded by approximately 250 watts at the low end and about 350 watts at the high end. Within this broad range, there is a narrower range of up to 25 watts (less than that at end-of-life) over which the so-called multiple operating points can occur. Location of the narrow range within the broad range is dependent on the time of life and state of charge of the eight batteries in the system. The overall effects of the multiple-operating-point phenomenon are not serious in the Nimbus B power subsystem, because:

- First, chances of the occurrence of the multiple operating points at end-of-life are very small, at least under the conditions of the assumed component characteristics.

- Second, the effect of an undesirable operating point is merely a moderate decrease in the recharge rate.

- Third, the effect apparently cannot occur until several batteries are in trickle charge, which occurs normally upon full recharge.

Finally, an outdoor illumination test of the two Nimbus solar panels was conducted to establish whether all the multiple operating points indicated by a graphical analysis of the load lines are stable and practically possible. The solar-panel electrical output was connected to the remainder of the power subsystem, and a variable load was delivered by an AVR. During the test, condition of all batteries in trickle charge was simulated in order to make it possible for the multiple operating points to occur.

Figure 17 illustrates the results of this test, where a-b-c-d is recognized as the output characteristic analogous to d-o-t-h in Figures 14, 15 and 16. Stable operating points achieved during the test depended upon the load magnitude and the direction of the load change, as shown in Figure 17. With a load adjusted to a magnitude less than P_x, the operating point was located along the reflected voltage limiter characteristic c-d. Adjusting the load magnitude upwards to P_y, the operating point moved along c-d, up to point c. Slight load increase above P_y caused the operation to switch from c to a as shown by the

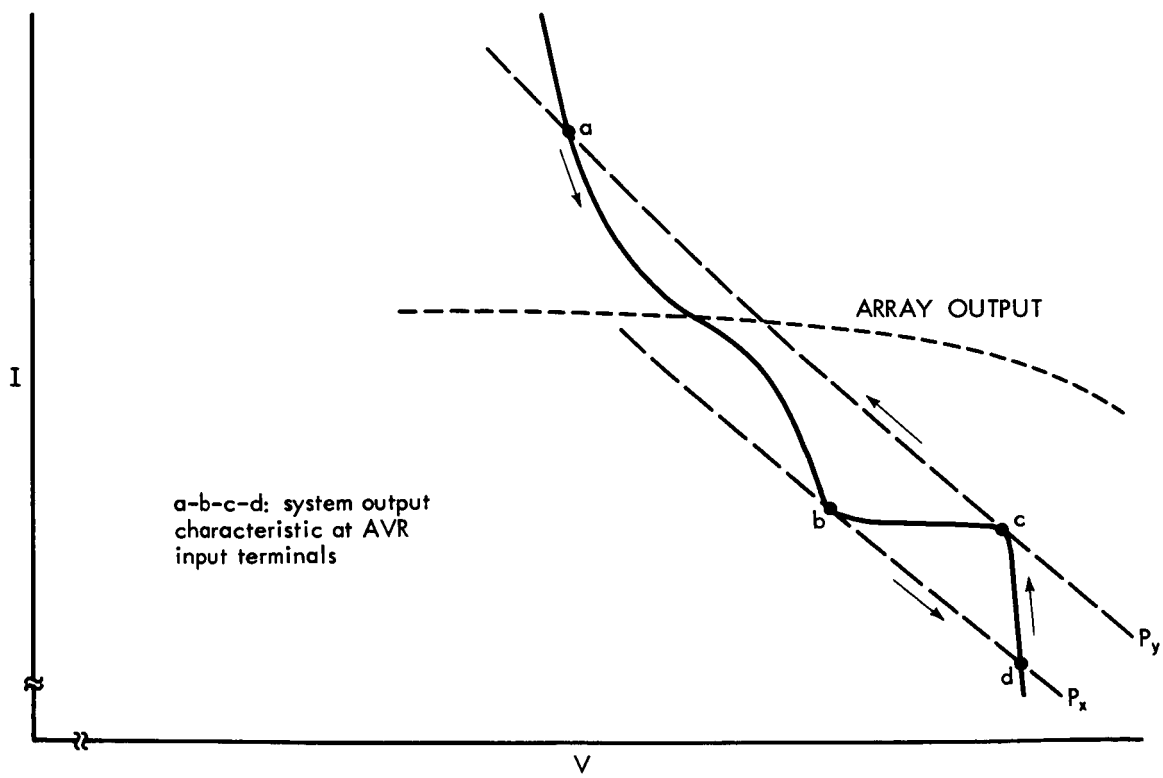

Figure 17. Stable Operating Points

arrow. Following that, the load was again reduced, and the operating point moved downwards along a-b. Reduction below P_x resulted in switching the operating point from b to d.

The apparent hysteresis effect observed experimentally can be described quantitatively as covering a range of about 6 or 7 volts along the voltage axis, and occurring over a load range of approximately 22 watts. Stable operating points such as b' (Figure 16) could not be achieved.

ADVANCED CONCEPTS

The Nimbus orbit has a repetitive 35-minute satellite night and a 73-minute satellite night. As the satellite leaves the dark, it emerges into the sun with a solar array temperature of -74° C and heats up to a maximum of approximately +50° C. The output characteristic of the solar cells causes the maximum power point of the solar array to decrease proportionally to the increase in temperature. This change in maximum power point with temperature takes place at a relatively constant current.

In the conventional system, the battery voltage fixes the voltage operating point on the array. The location of the operation point must provide sufficient voltage to charge the batteries with the warm solar array, and the system therefore will not permit taking advantage of the increased power at the colder temperatures of the solar array.

Implementation of a maximum power-point tracker, however, will permit operation on the maximum power point of the solar array throughout the entire daytime portion of the orbit. This increase in available power is contrasted by the dashed line for the maximum power point and the solid line for the conventional system in Figure 18.

This section describes maximum power-point tracking technology and evaluates it for possible use in the third-generation Nimbus spacecraft power subsystem. The three methods of tracker implementation are the series tracker, the parallel tracker, and the part-time parallel tracker, and all three are compared to the Nimbus B system on a performance basis. Comparisons are made to determine the ability of each to maintain the spacecraft in a state of energy balance, over a broad range of electrical loads, rather than for a specific load power profile.

The block diagram in Figure 19 shows a two-module series tracker, but it is understood that many more modules can be involved.

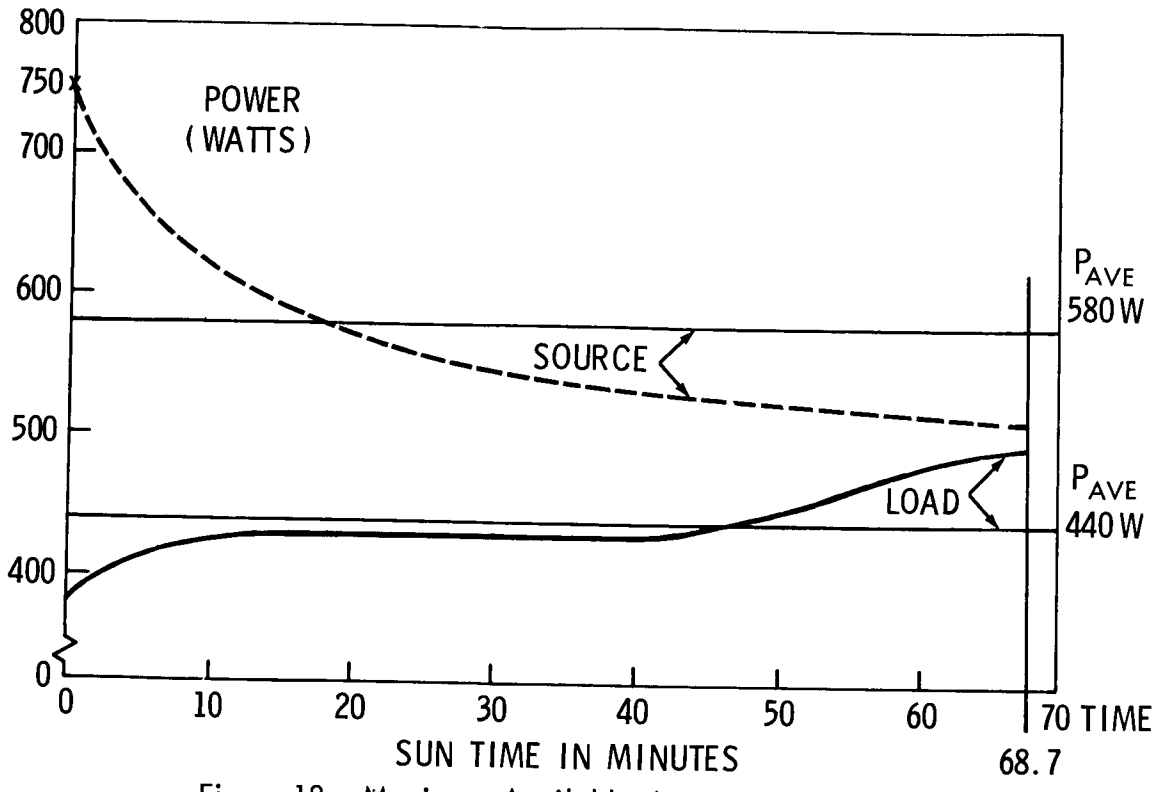

Figure 18. Maximum Available Array Power Used by a Conventional Power System vs Sun Time

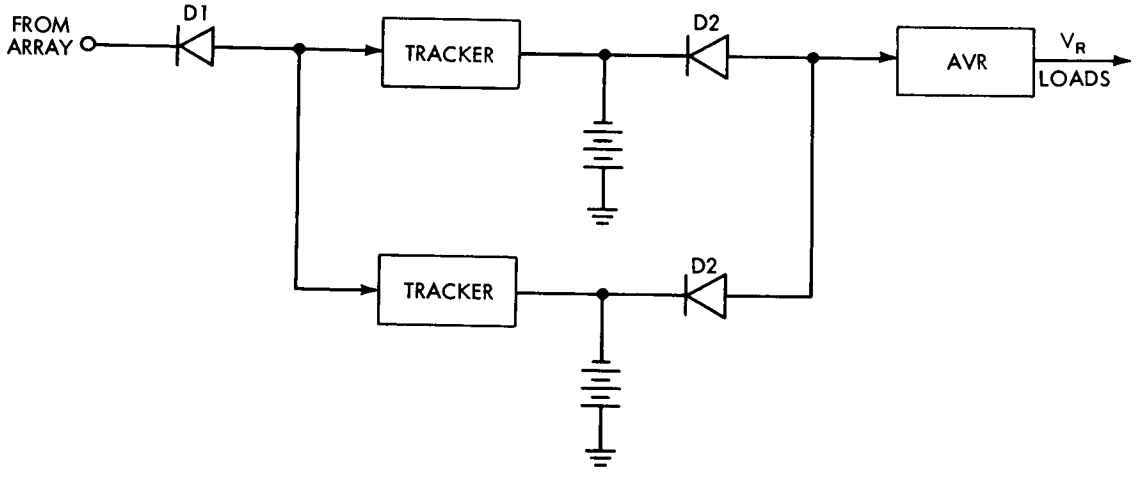

Figure 19. Series-Tracker Power System

The pulsewidth-modulated (PWM) regulator which seeks and locks on to the maximum power point of the solar array (i.e., the tracker) is placed in series with the array. V_{max} , I_{max} of the array appears at the tracker input at all times (less allowance for line losses), regardless of the load magnitude at the regulated bus voltage V_R. The series-tracker output voltage is determined by the battery, but the product of the tracker output voltage and current is equal to (V_{max}) (I_{max}) of the array, times a more or less fixed efficiency factor of the tracker. The series-tracker output is thus equal to the P_{max} of the solar array at any time, less unavoidable losses; the tracker system of this type is full-time, because P_{max} is tracked at all times regardless of the load magnitude.

The series-tracker output is shared by the battery, and by the AVR input requirement determined by the instantaneous load. If the battery charge becomes excessive, the tracker output is reduced.

Figure 20 is a diagram of a two-module full-time parallel tracker. In this system, the tracking device is placed in a series with the battery; the series combination is electrically in parallel with the array and the load. A parallel tracker maximizes the power difference between the array output and the load requirement during charge; the array V_{max} thus appears at the tracker input,

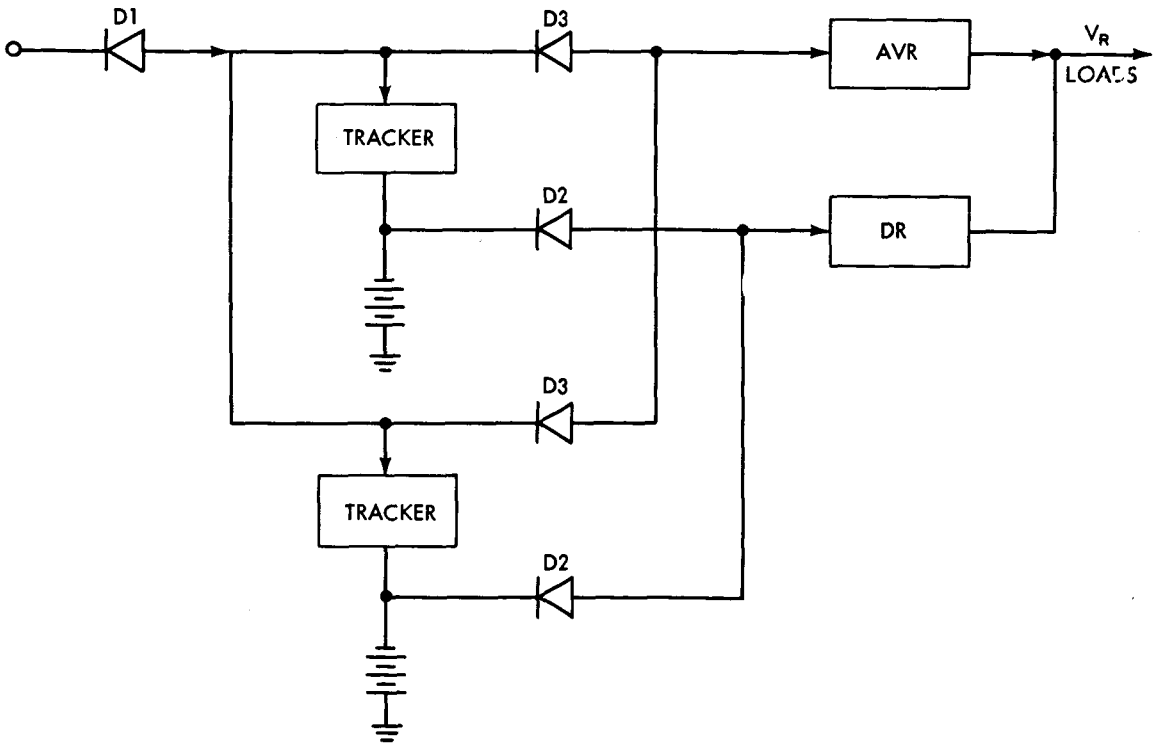

Figure 20. Full-Time Parallel-Tracker System

as in the series tracker. During daytime battery discharge, V_{max} is maintained, causing maximum array power (less line losses) to be delivered to the load through the AVR. The required power difference (as during a peak load) is taken from the battery through the discharge regulator (DR).

The full-time parallel-tracker system is designed so that the battery discharge during a daytime peak load is minimized. Even though the tracker unit is no longer active during discharge, the AVR will itself seek the array P_{max} and maintain its input at roughly the array V_{max} voltage. Maximum array output is thus drawn first, before the battery is allowed to discharge, and the lowest possible battery discharge is therefore assured. As in the series tracker battery charge is reduced in this system when required.

The part-time parallel-tracker operation is in every way identical with that of the full-time parallel tracker, as long as the power system remains in "charge." During discharge, however, the array V_{max} voltage can no longer be maintained, and the system operates in the nontracking mode as it does in the present NIMBUS B.

In the part-time tracker, the battery-discharge path (thru D2 diodes) is connected to the AVR input; since there is no discharge regulator, isolation between the AVR input and the battery-discharge voltage can no longer be maintained as it was in the full-time parallel tracker. Consequently, in the part-time tracker, the AVR input voltage is roughly equal to the battery voltage when in discharge, usually several volts removed from the array V_{max}.

It is necessary to compare the relative performance of these three tracker systems with that of the Nimbus B power system. For our purposes we will assume that the most desirable performance is achieved when the battery charge is maximized (or, when battery discharge is minimized) for any given fixed conditions of load and array temperature. With this approach adopted as a standard of quality, the method of comparison consists of plots of battery current vs load for each of the four systems compared.

Several assumptions must be made: First, the comparison will be limited to end-of-life conditions. Second, it will be assumed that the array and battery characteristics of the tracker systems are as in Figures 11 and 12, but that the average efficiency factor of all PWM devices used in the tracker systems (tracker units, DR, and AVR) is 0.9. Third, assume that the Nimbus B performance at end-of-life is as in Figure 14, where Figure 8 has been used to reflect true AVR efficiency variation with load and input voltage (precise efficiency data for the AVR and other PWM devices are not available in a tracker application). Fourth, assume the following similarities between the tracker

systems and Nimbus B: there will be eight battery modules; the shunt current losses at the regulated, unregulated, and battery voltage levels will be as measured on the Nimbus B power subsystem; the line drops will be 1.8 volts through D1 path, 0.45 volts through D2, and 0.35 volts through D3 (Figures 19, 20, and 21).

A sample calculation will produce plots as shown in Figure 22, using the series tracker as a model. The solar-cell output at steady-state solar-array temperature is 38 volts and 9.52 amperes: that is, the location of the array P_{max} in Figure 12. Tracker input will equal that, less the voltage drop through D1, i.e., 36.2 volts (9.52 amps) = 345 watts; tracker output, 345 (0.9) = 310 watts.

As an example, assume a total charge current of 4 amperes (0.5 amp/battery); from Figure 11, the storage cell voltage corresponding to 0.5 amps charge is 1.366 volts, or 31.42 volts across a 23-cell battery. The tracker output current will equal 310 watts divided by 31.42 volts, or 9.86 amperes.

The AVR input current I_o, given a 4-ampere total charge, will equal (9.86 -4) amperes less the total shunt loss of 0.352 amperes (sum of losses at battery

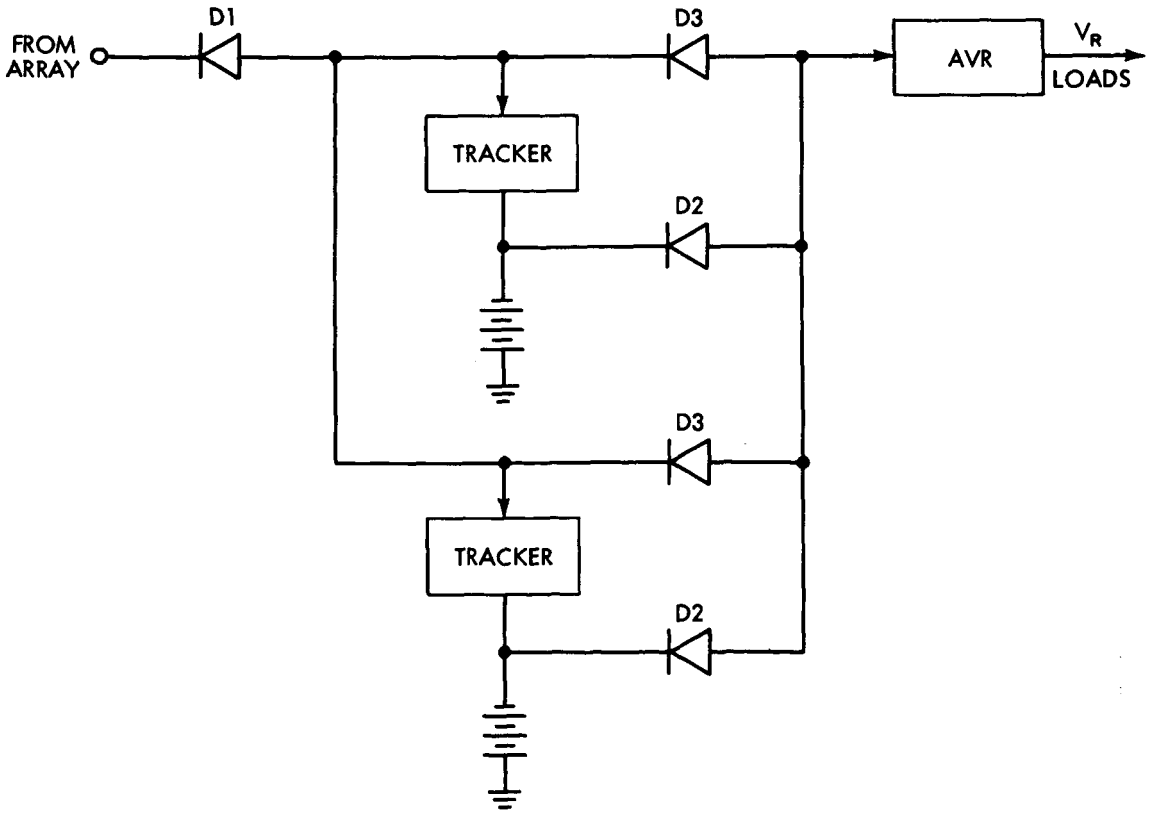

Figure 21. Part-Time Parallel-Tracker System

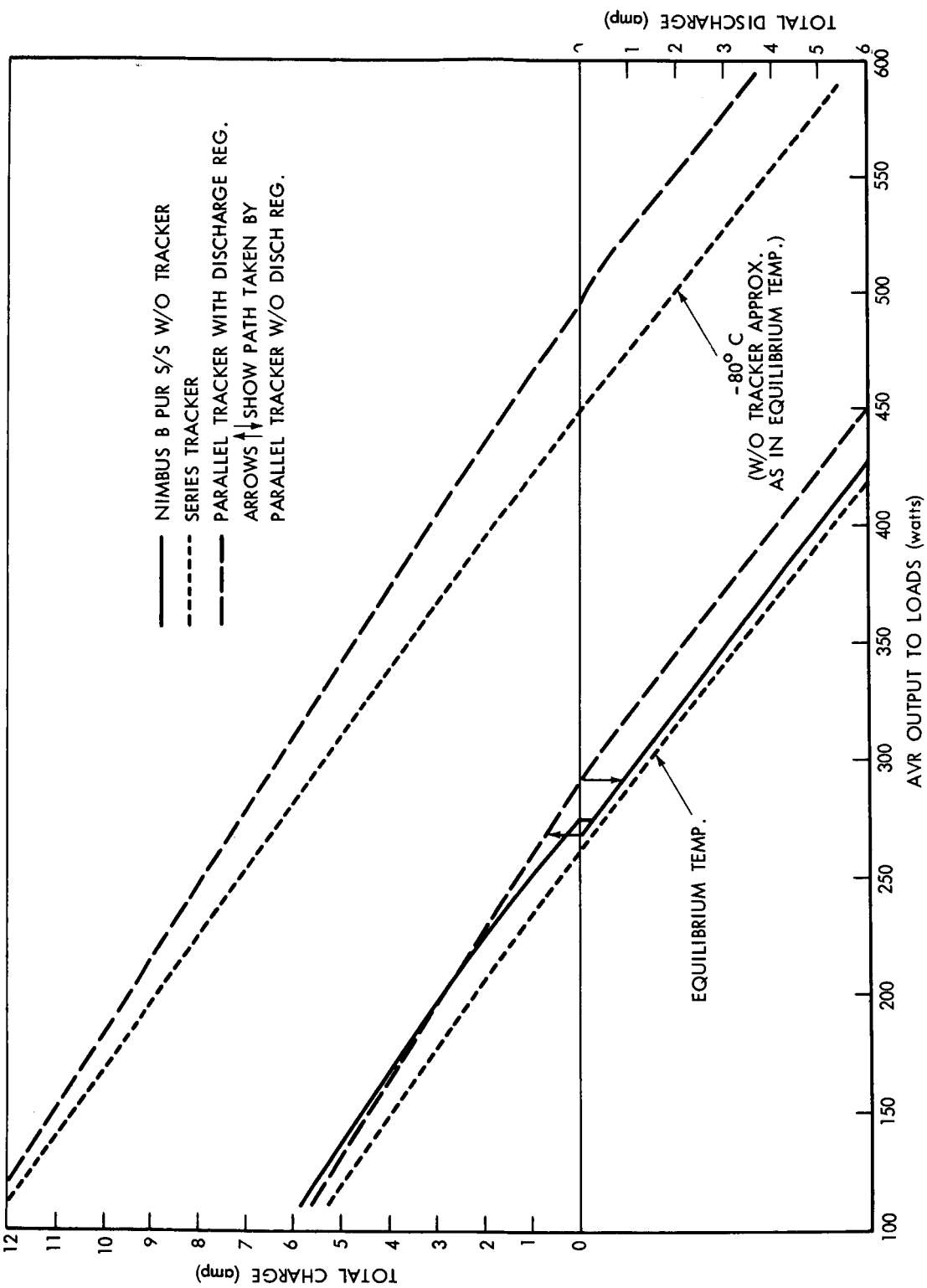

Figure 22. Performance Comparison of Tracker Systems

and unregulated bus voltage), or 5.51 amperes. The AVR input voltage V_o equals 31.42 volts less drop through the D2 path, or 30.97 volts. Load delivered by the AVR equals the Product $V_o I_o$ times the assumed efficiency factor 0.9, less 5 watts shunt loss incurred at the regulated bus voltage level; net load magnitude is 148.5 watts in this case.

The series-tracker system plot in Figure 22 contains a point described by 4 amperes charge and 148.5 watts load, at steady-state solar-cell temperature. By comparison, Figure 22 shows that the present Nimbus B system, as well as a parallel-tracker system, would deliver a 4.5-ampere charge for the same load condition; the series-tracker system here appears at a disadvantage.

Let the discharge mode be examined: Assume a series-tracker system where the total battery-discharge current is 2 amperes, or 0.25 amps/btry. From Figure 11, the battery-discharge voltage is 29.64 volts in a 23-cell battery configuration. Assuming sun-illuminated panels at steady-state temperature, the net tracker output will be 310 watts, the same as in the charge mode. Tracker output current will be 310/29.64 = 10.44 amperes.

The AVR input current is the sum (10.44 + 2) amperes, less the shunt loss, or 12.09 amperes at AVR input terminals. The input voltage V_o will be the battery-terminal voltage reduced by the drop through the D2 path, or 29.19 volts. Net AVR output power will equal (12.09) (29.19) (0.9) -5 = 312 watts. Figure 22 shows the 312-watt load condition corresponding to a 2-ampere discharge in a series-tracker system, which is 0.2 amperes more than in Nimbus B and approximately 1.2 amperes more than in a full-time parallel tracker.

Figure 23 shows temperature time profiles of the two Nimbus panels, obtained from in-flight telemetry data of the Nimbus C spacecraft. Both extremes of the array temperature are considered in Figure 22: i.e., the coldest predicted (approximately -80° C), and +40° C corresponding roughly to the steady-state, or thermal equilibrium temperature. The two states of the array output result in two families of battery current-vs-load plots.

Plots shown in Figure 22 have been prepared using Nimbus B power subsystem characteristics, and are thus believed to provide a fair basis of comparison for planning future Nimbus missions.

The Nimbus B system performance shown in Figure 22 has been transcribed from Figure 14. Even though the solid-line plot shown applies to a +40° C array temperature, it can be assumed that colder array temperatures would not greatly influence the location of that plot along the abscissa.

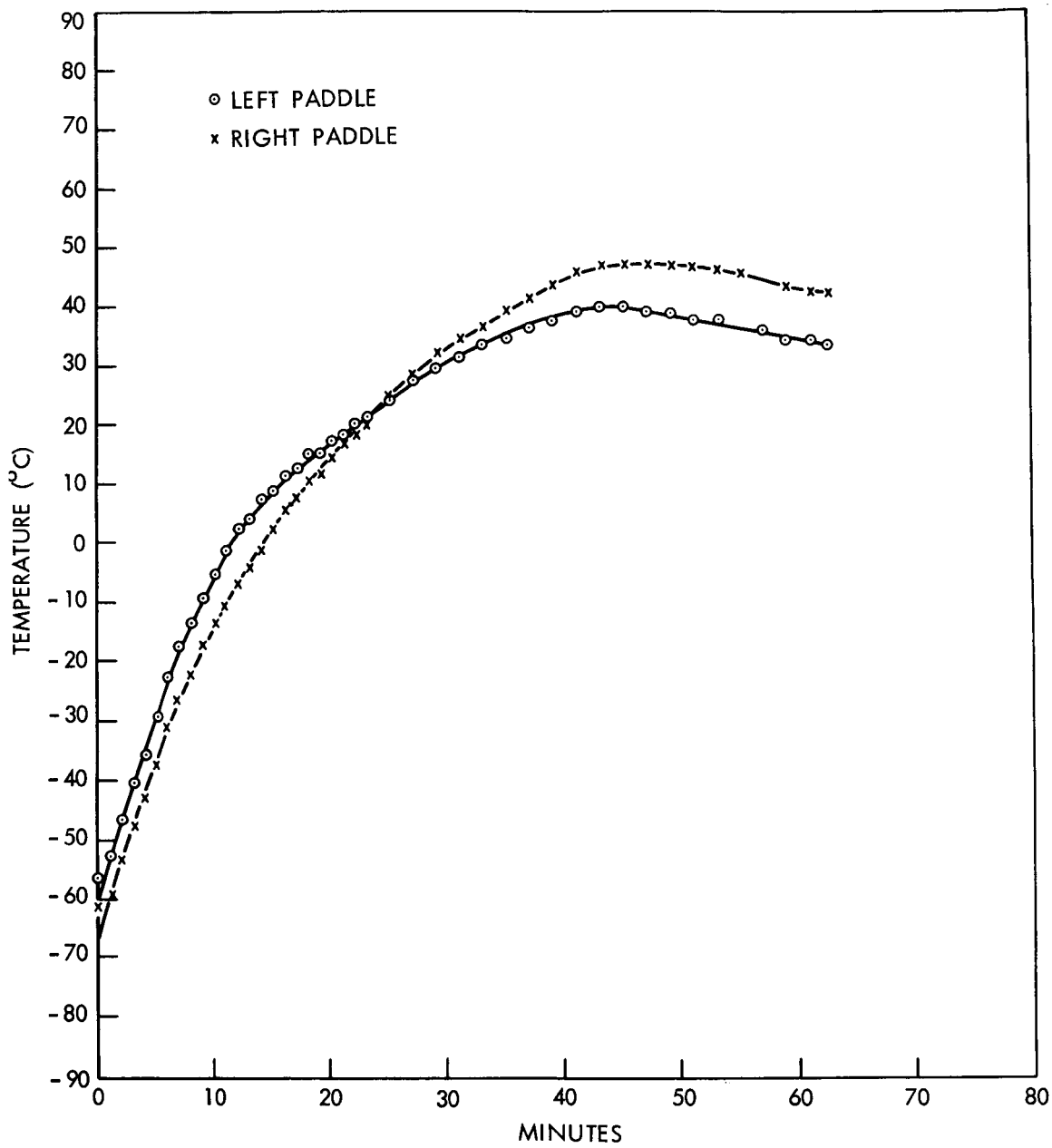

Figure 23. Nimbus C Second Orbit, Daytime Array Temperature

The tracking system performance, on the other hand, is greatly influenced by the array temperatures as shown. The plot clearly shows the superiority of a tracking system, in that it can take advantage of the increased array power during the temperature transient by being able to supply a much larger total charge current for a time, given a fixed load requirement. During steady-state array temperature, however, a tracking system shows less of an advantage over a well-designed conventional nontracking approach.

A significant conclusion drawn from Figure 22 is that a parallel tracker is always more efficient (i.e., it applies more charge, draws less discharge) than the series tracker, regardless of the load magnitude or the array temperature. This conclusion is unavoidable considering that, in the series approach, all the array power is subject to the tracker inefficiency, whereas in the parallel tracker only the battery charge is subjected to that loss. The most significant advantage of the series-tracker approach is that it is the simplest system with a full-time tracking capability.

The part-time parallel tracker behaves the same way as the full-time parallel tracker when in "charge." During equilibrium temperature, Figure 22 shows both types of parallel tracker continuing together up to a load of about 291 watts; with a slightly higher load, the part-time tracker drops out of the tracking mode, as shown by the arrow pointing downwards to the plot of the nontracking Nimbus B system, and continues along the latter plot for all higher loads. Then, if the load is decreased, the part-time tracker follows the nontracking plot until zero discharge condition is reached. The graph shows this to correspond to about 268 watts load. A further slight load decrease causes the system to resume tracking; added power suddenly released by the array is delivered as a step charge to the battery, as shown by the upward-pointing arrow.

The full-time version of the parallel tracker requires the complexity of a discharge regulator to maintain isolation between the AVR input and the battery bus, as well as sensing and logic circuitry to turn it on at the proper time and to keep it off during the charge cycle. The part-time tracker is, therefore, a much simpler approach, and the final tradeoff should be based on the duration of the discharge anticipated during daytime and on the timing of the peak load causing the discharge.

In summary, it can be said that at end-of-life, a parallel tracker would provide nearly 1 ampere-hour more recharge per orbit than a series tracker. This is a considerable advantage, in view of the fact that the total recharge per orbit at end-of-life is of the order of 5 ahrs. Although the full-time parallel tracker will perform better, given a perfectly general application, the performance improvement over the part-time tracker will be slight unless long-duration peak loads are present. If there are no peak loads during daytime, the two will perform equally well; if the peak loads are short-duration, and particularly if they occur during the latter part of the satellite daytime, the difference will be small.

Considering the aforesaid, either type of parallel tracker appears to offer definite advantages over either the series tracker or the present Nimbus B approach.